Operational Mechanism of Conjugated Polyelectrolytes

ARTICLE *in* JOURNAL OF THE AMERICAN CHEMICAL SOCIETY · MAY 2014

Impact Factor: 12.11 · DOI: 10.1021/ja502055x · Source: PubMed

7 AUTHORS, INCLUDING:

Daniel Tordera
Linköping University
36 PUBLICATIONS **562** CITATIONS
SEE PROFILE

M. Kuik
University of California, Santa Barbara
34 PUBLICATIONS **695** CITATIONS
SEE PROFILE

Enrico Bandiello
University of Valencia
10 PUBLICATIONS **93** CITATIONS
SEE PROFILE

Henk J. Bolink
University of Valencia
208 PUBLICATIONS **4,905** CITATIONS
SEE PROFILE

JACS
JOURNAL OF THE AMERICAN CHEMICAL SOCIETY

Communication

pubs.acs.org/JACS

Operational Mechanism of Conjugated Polyelectrolytes

Daniel Tordera,[†,‡] Martijn Kuik,[†] Zachary D. Rengert,[†] Enrico Bandiello,[‡] Henk J. Bolink,*[,‡] Guillermo C. Bazan,*[,†,§] and Thuc-Quyen Nguyen*[,†]

[†]Department of Chemistry & Biochemistry, Department of Materials, and Center for Polymers and Organic Solids, University of California, Santa Barbara, California 93106, United States

[‡]Instituto de Ciencia Molecular, Universidad de Valencia, C/ Cat. J. Beltran 2, ES-46980 Paterna, Spain

[§]Center of Excellence for Advanced Materials Research (CEAMR), King Abdulaziz University, Jeddah, Saudi Arabia

Supporting Information

ABSTRACT: Conjugated polyelectrolytes (CPEs) are versatile materials used in a range of organic optoelectronic applications. Because of their ionic/electronic nature, characterizing these materials is nontrivial, and their operational mechanism is not fully understood. In this work we use a methodology that combines constant-voltage-driven current-density transient measurements with fast current vs voltage scans to allow decoupling of ionic and electronic phenomena. This technique is applied to diodes prepared with cationic CPEs having different charge-compensating anions. Our results indicate that the operational mechanism of these devices is governed by electrochemical doping of the CPE. On the basis of the notion that the saturated depletion layer for the anions consists of the same π-conjugated backbone material, we discern how the extent and speed of formation of the doped region depend on the anion structure. Apart from addressing fundamental transport questions, this work provides a tool for future characterization of different CPEs and other similar systems.

Conjugated polyelectrolytes (CPEs) are macromolecules that contain an electronically delocalized backbone and solubilizing side groups with ionizable functionalities.[1] CPEs are therefore soluble in polar solvents[2] and combine the dependence of polyelectrolytes on electrostatic forces with the properties of organic semiconductors. As a result of these unique properties, CPEs have been extensively applied in biosensors[3,4] and single-component light-emitting electrochemical cells (LECs)[5] and as interfacial layers in multilayer polymer light-emitting diodes (PLEDs),[6−8] organic photovoltaics,[9,10] and field-effect transistors.[11] There are reports on the operational principles when CPEs are used as thin electron injection/transport layers on PLEDs.[12−14] When the CPE layer is thick, there can be a redistribution of ions within the CPE layer and hole accumulation at the CPE/electroluminescent layer interface.[12] However, the precise effect of ionic movement on key charge-transport properties remains poorly understood. These uncertainties are mainly due to the difficulty in decoupling the electronic and ionic contributions to device currents. Applying a voltage induces movement of the ions; thus, the equilibrium state of the device changes. As a result, current density−voltage (J−V) scans show hysteresis that depends on the scan rate.[15,16]

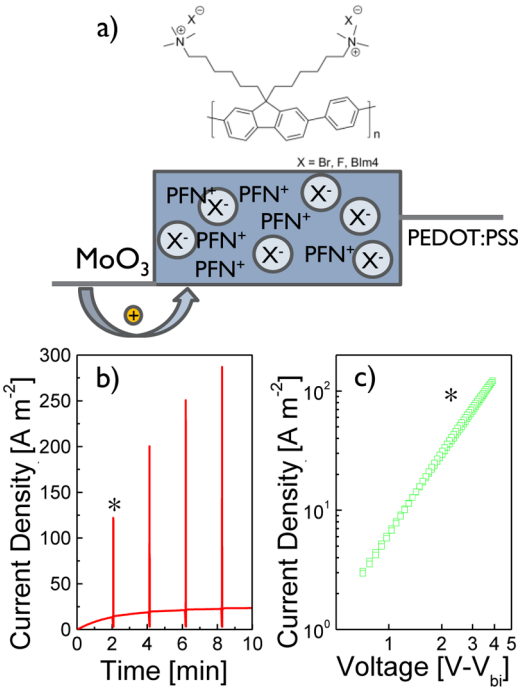

Figure 1. (a) Chemical structure of PFN^+X^- and schematic design of the device configuration. (b) Current-density transient of the CPE PFN^+F^- driven at 2.5 V. The vertical lines at 2 min intervals correspond to the current density of the J−V scans performed during the operation of the device. (c) Fast J−V scan (6 V/s). The asterisk depicts the correlation between panels b and c.

Characterizing electrical properties, such as mobility, from these scans is not trivial, as the data are influenced by both ionic and electronic effects. Pulsed bias technique has been used to suppress ion motion in single-carrier diodes.[13]

In this work we apply a methodology that combines constant-voltage-driven current-density transient measurements with fast current vs voltage scans to allow for decoupling of the ionic and electronic contributions.[17] Three different CPEs with the same backbone and different counterions were evaluated using hole-only diodes. Incorporating different counterions allows us to postulate that not only the ionic mobility is important but also

Received: February 27, 2014

   dx.doi.org/10.1021/ja502055x | J. Am. Chem. Soc. XXXX, XXX, XXX−XXX

the ionic dissociation probability. The data allow us to show evidence for the formation of an electrochemically doped layer and to estimate the extent of these doped zones. Finally, the effect of the different counterions is analyzed with respect to differences in the extent of the doped regions and the relative mobility of the ions and their stability.

Hole-only devices (Figure 1a), used as the primary test bed, were fabricated as follows. Indium tin oxide (ITO)-coated glass plates were cleaned with soap and successive sonication in water, 2-propanol, and acetone baths. After drying, the substrates were placed in a UV-ozone cleaner for 30 min. A 35 nm layer of poly(3,4-ethylenedioxythiophene):poly(styrenesulfonate) (PEDOT:PSS) was spin-coated on the ITO glass substrate to improve the reproducibility of the devices and to prevent pinhole formation. The substrates were then transferred into an inert atmosphere glovebox, and films consisting of poly[9,9′-bis-[6″-(*N*,*N*,*N*-trimethylammonium)hexyl]fluorine-*alt*-*co*-phenylene] (PFN^+) with tetrakis(imidazolyl)borate (BIm_4^-), bromide (Br^-), or fluoride (F^-) counteranions were spin-coated from 30 mg/mL methanol solutions at different speeds, resulting in films of thickness from 215 to 455 nm. Finally, using a shadow mask, a 10 nm molybdenum oxide (MoO_3) electrode topped with a 100 nm aluminum layer was evaporated under vacuum ($<1 \times 10^{-6}$ mbar). The area of the device was 4.5 mm^2. Devices were not encapsulated and were characterized under nitrogen at room temperature.

Initial experiments involved *J*−*V* measurements carried out at a fast rate (6 V/s). Even under these conditions, one observes hysteresis of the *J*−*V* curves. To circumvent this, in analogy to the work presented by Lenes et al.,[17] we maintained a minimum voltage over the device such that the voltage sweeps are performed in an up−down−up sequence (Figure 1b). No hysteresis is observed in the *J*−*V* sweeps measured in this way, either for the as-cast samples or after application of a fixed voltage. From Figure 1b, the current density obtained at the set fixed voltage before and after a *J*−*V* scan is exactly the same, a further indication that ions do not significantly move during the scan. As observed previously for ionic liquids, applying a constant voltage leads to different *J*−*V* sweeps, which has been related to the movement of ions. The above-described protocol works best with layers at least 200 nm thick, as this increases the resolution between ionic and electronic contributions to the current.[18] As a final note on experimental details, the choice for contact materials is important and influences charge carrier injection, similar to what has been shown for ordinary ion-free organic semiconductors.[19]

The effect of three counterions ($X^- = BIm_4^-$, Br^-, and F^-) on the charge transport of PFN^+X^- was investigated. Hole-only devices with the structure ITO/PEDOT:PSS/PFN^+X^-/MoO_3 were prepared. MoO_3 was selected as the hole-injecting electrode due to the deep HOMO of PFN^+X^- (~5.8 eV),[20] which is similar to that of the neutral counterpart, poly(9,9-dioctylfluorene) (PFO). In PFO it was shown that MoO_3 forms a truly ohmic contact.[19] For the devices prepared above, one observes that the rectification is independent of the direction of the initial *J*−*V* sweep (Figure S1). This suggests that, regardless of the preconditioning, the PEDOT:PSS contact remains injection limited, most likely due to the initial contact barrier. Hence, the choice for contact materials is vital in order to discern the various transport mechanisms. For this reason, in this work we investigate injection only from MoO_3 (see Figure 1a).

Figure 2 shows the current-density transient and selected *J*−*V*'s for a 265 nm $PFN^+BIm_4^-$ device driven at 3.5 V. The general

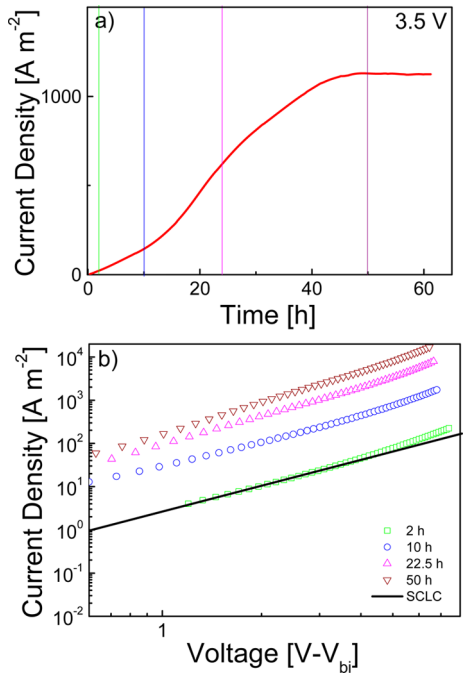

Figure 2. (a) Current-density transient for a $PFN^+BIm_4^-$ device driven at a constant voltage of 3.5 V. *J*−*V* scans are performed at time intervals indicated by the vertical lines. (b) Resulting *J*−*V* plots for the same device taken at the selected times.

characteristics of these data are observed for the other materials and applied voltages and are provided in the Supporting Information (SI). One observes that the current-density transient increases over time until it reaches a steady state after ~45 h. *J*−*V* measurements were performed at the beginning of the transient measurement (2 h), during the increase of the current density (10 and 22.5 h), and when the current-density saturation was reached (50 h); the results of these experiments are shown in Figure 2b. After correction for the V_{bi},[17,21] one finds a quadratic dependence and that V_{bi} increases from 1 to 1.4 V. The initial value is consistent with the energetic offset between the CPE HOMO and the PEDOT:PSS work function, while the increase to 1.4 V is attributed to the buildup of positive ions at the PEDOT:PSS active layer interface. It is worth noting once more that thicker CPE layers suffer less from contact effects. Hence we observe less influence of the V_{bi} for thicker layers. Very similar behavior is observed for the devices using CPEs with Br^- and F^- counterions (Figures S2−S4).

Figure 2a shows that even though the applied voltage is kept constant, an increase in the current density is observed. Since there is an ohmic contact for hole injection, the resistivity of the PFN^+X^- layer must be decreasing with time. A similar effect has been observed in other ionic/electronic systems, such as polymeric or ionic transition-metal complex LECs.[17,22] In those systems the increase in current density at fixed operation voltage was attributed to the formation of highly conductive doped regions adjacent to the electrodes. By analogy, it appears likely that a similar phenomenon occurs in PFN^+X^- hole-only devices. It is probable that, under the constantly applied voltage, a fraction of the counteranions migrate toward the positively charged contact. Hole injection can be viewed as oxidation of the conjugated backbone and formation of positive polarons (radical cations). The presence of excess mobile anions near the anode leads to Coulombic stabilization of the polarons. This process is

dx.doi.org/10.1021/ja502055x | *J. Am. Chem. Soc.* XXXX, XXX, XXX−XXX

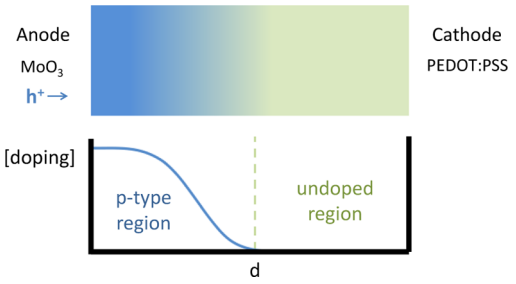

Figure 3. Schematic representation of the proposed operational mechanism under steady-state conditions.

known as electrochemical doping and leads to the formation of highly conductive regions. The applied voltage now mainly drops over the intrinsic (nondoped) region of the PFN^+X^- layer, causing more ion dissociation and migration.[23] Hence, with constant voltage driving, the doped regions grow with time (assuming that the anions are available to compensate injected holes). This is observed in the J vs time plot as a gradual increase in J. However, J reaches a plateau after a certain time of operation. At that time it can be assumed that PFN^+X^- has reached its maximum doping level (Figure 3).

The quadratic dependence allows us to investigate the $J-V$ curves. The hole mobility extracted at $t = 0$ is 2×10^{-9} m^2 V^{-1} s^{-1} for PFN^+F^-. This value is the same as that of PFO (2×10^{-9} m^2 V^{-1} s^{-1})[19] and will be used to calculate the doped region. Correcting for an effective thickness for an ion-doped depletion layer, the Mott–Gurney law reads

$$J = \varepsilon_0 \varepsilon_r \mu_0 \frac{(V - V_{bi})^2}{(L - L_d)^3} \quad (1)$$

where $\varepsilon_0\varepsilon_r$ is the dielectric constant, μ_0 the zero-field mobility, V the applied voltage, L the active layer thickness, and L_d the correction for the doped ion depletion layer. Deviations at high voltages of the quadratic nature of the space-charge limited current (SCLC) can be attributed to the field effects on the mobility.[24] The assumption of a discrete depleted layer and a sharply edged doped layer is clearly a simplification that only might approach reality for the saturated current case. However, it can be observed that under these assumptions the current–voltage characteristics show space-charge behavior, which suggests that the depletion undoped layer can be regarded as an effective layer thickness.

Interestingly, as the doped region does not limit the transport, if the mobility of the intrinsic layer is known, the extent of the doped region can be estimated using the Mott–Gurney law (eq 1). For a 265 nm $PFN^+BIm_4^-$ device driven at 3.5 V, the thickness of the doped region, L_d, increases over time, reaching 180 nm, which is 70% of the total active layer. When the device is in steady state, V_{bi} is found to increase to ~1.4 V, which is likely a consequence of the fact that the already present energy offset between the PEDOT:PSS and the HOMO of the $PFN^+BIm_4^-$ is ~1.0 eV and increases due to the electrostatic presence of the positively charged ionized PFN^+ for a saturated device.

The same 265 nm $PFN^+BIm_4^-$ device driven at a constant voltage of 4.5 V with $J-V$ scans at different intervals of time has also been studied (Figure S2). Similar to the aforementioned analysis of the $PFN^+BIm_4^-$ device driven by a constant voltage of 3.5 V, when the device is driven at 4.5 V the current-density transient increases over time until reaching a steady state (followed by a decrease of the current density caused by possible

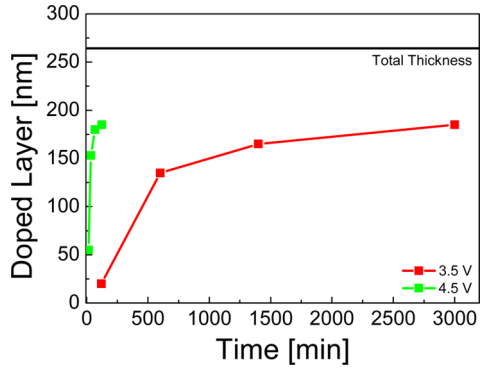

Figure 4. Evolution of the thickness of the doped region vs time for $PFN^+BIm_4^-$ devices driven at different voltages.

degradation of the material). The $J-V$ scans taken at different times during this operation all show SCLC behavior and can thus also be fitted using the Mott–Gurney law. As previously, using a mobility of 2×10^{-9} m^2 V^{-1} s^{-1} and V_{bi} = 1.4 V allows us to determine the evolution of the doped layer thickness vs time. In Figure 4, the evolution of L_d vs operation time is presented for the devices using $PFN^+BIm_4^-$ driven at 3.5 and 4.5 V. The L_d saturates at ~180 nm (70% of the total thickness), indicating that the thickness of these doped regions is independent of the voltage used to drive the devices.

Devices based on 455 nm thick PFN^+Br^- layers were studied at different voltages (2.5, 3, and 3.5 V). The current-density transients and selected $J-V$'s are shown in Figure S3. The current-density transients are similar to those for $PFN^+BIm_4^-$ devices. However, PFN^+Br^- diodes show a rapid decrease in current after achieving a steady state, even when operated at voltages as low as 2.5 V. This indicates that PFN^+Br^- is less stable than $PFN^+BIm_4^-$, which is consistent with literature precedent using PFN^+Br^- as an electron injection layer in PLEDs.[25] With this in mind, V_{bi} = 1.4 V is also obtained and the extent of the doped zone is calculated, resulting in L_d = 365 nm (80% of the total thickness of the active layer). Similarly, 215 nm devices containing PFN^+F^- were also studied at different voltages (2.5, 3, 4, and 4.5 V). Both current-density transients and selected $J-V$'s are shown in Figure S4. Again, using a mobility of 2×10^{-9} m^2 V^{-1} s^{-1}, the same V_{bi} = 1.4 V is found. In this case the extent of the doped zone reaches 90 nm, or 40% of the total thickness of the active layers. The stability of PFN^+F^- appears to be best, as no decrease in current density is observed for voltages up to 4 V. The evolution of the L_d vs time for the different voltages for both anions, Br^- and F^-, can be found in Figure S5. The final thickness of the doped zone is the same for each anion, regardless of the voltage applied (except for the case of the PFN^+F^- device driven at 2.5 V, where the steady state is not reached). The time it takes to reach the total extension of the doped zone decreases with increasing voltage, as expected.

The thickness of the doped region corresponds to 80%, 70%, and 40% of the total active layer thickness for Br^-, BIm_4^-, and F^-, respectively. The capacitance of the device was measured as a function of time using impedance spectroscopy. One would expect an increasing capacitance with doping. The evolution of the thickness of the device over time was calculated from the capacitance data. It is observed that, similarly to the $J-V$ analysis, the thickness of the intrinsic layer decreases over time from 212 to ~55 nm at the plateau, indicating a doped zone extension of 157 nm, or 74% of the total thickness of the active layer for the PFN^+Br^- devices, in good agreement with the value deduced

dx.doi.org/10.1021/ja502055x | J. Am. Chem. Soc. XXXX, XXX, XXX–XXX

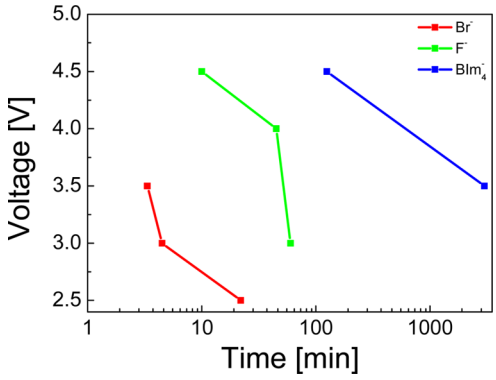

Figure 5. Time to reach the steady state vs voltage for the different X^- anions on PFN^+X^- devices.

from the $J-V$ analysis above (see SI for the impedance-derived data). The difference in L_d is not directly related with the size of the ions and could be ascribed to differences in the packing of these ions in the doped zone. The relative mobility of the different ions can be also highlighted by plotting the time to reach the steady state vs the voltage applied on the current-density transient (Figure 5). The relative speed decreases from Br^- to F^- to BIm_4^-. Once again, this mobility is not directly related to the size of the ions, where the trend $F^- > Br^- > BIm_4^-$ would be expected. This is a possible hint that not only the mobility but also the energy of dissociation play roles in determining the time to reach the steady state, i.e., the time to reach the maximum extended doped region.

In conclusion, combining constant-voltage-driven current-density transient measurements with fast current vs voltage scans provides insight into the operational mechanism of CPE diode devices. Evidence for the formation of electrochemically doped regions is obtained. The extent of the doped regions appears to be limited by the availability of uncompensated anions in the film. The relative mobility of the different anions has also been studied, indicating that both mobility and energy of dissociation play roles in determining the speed of formation of the doped zones. The stability of the CPE depends highly on the counteranion used, with F^- being the most stable anion among the ones studied. Finally, we note that the methodology used in these studies could be used for future characterization of CPEs and other mixed ionic/electronic systems.

■ ASSOCIATED CONTENT

Supporting Information

Figures showing $J-V$ scans coupled with current-density transient measurements for the different anions and voltages, evolution of the thickness of the doped region vs time, and impedance spectroscopy data. This material is available free of charge via the Internet at http://pubs.acs.org.

■ AUTHOR INFORMATION

Corresponding Authors

henk.bolink@uv.es
bazan@chem.ucsb.edu
quyen@chem.ucsb.edu

Notes

The authors declare no competing financial interest.

■ ACKNOWLEDGMENTS

D.T. acknowledges the Spanish Ministry of Education, Culture and Sport for an FPU grant. Z.R. acknowledges UCSB for a Doctoral Scholars Fellowship and NSF for a Graduate Student Research Fellowship. This work is supported by a National Science Foundation CAREER grant (DMR-0547639) and the Spanish Ministry of Economy and Competitiveness (MINECO) (MAT2011-24594). E.B. acknowledges MINECO for an FPI grant. M.K. thanks the U.S. Department of Energy, Office of Basic Energy Sciences (DE-FG02-08ER46535), for support.

■ REFERENCES

(1) Hoven, C. V.; Garcia, A.; Bazan, G. C.; Nguyen, T.-Q. *Adv. Mater.* **2008**, *20*, 3793.
(2) Hu, S.; Zhong, C.; Wu, H.; Cao, Y. In *Conjugated Polyelectrolytes*; Wiley-VCH Verlag GmbH & Co. KGaA: Weinheim, Germany, 2012.
(3) Wang, D.; Gong, X.; Heeger, P. S.; Rininsland, F.; Bazan, G. C.; Heeger, A. J. *Proc. Natl. Acad. Sci. U.S.A.* **2002**, *99*, 49.
(4) Kahveci, Z.; Martínez-Tomé, M. J.; Mallavia, R.; Mateo, C. R. *Biomacromolecules* **2013**, *14*, 1990.
(5) Tsai, C.-S.; Yang, S.-H.; Liu, B.-C.; Su, H.-C. *Org. Electron.* **2013**, *14*, 488.
(6) Huang, F.; Wu, H.; Wang, D.; Yang, W.; Cao, Y. *Chem. Mater.* **2004**, *16*, 708.
(7) Fang, J.; Wallikewitz, B. H.; Gao, F.; Tu, G.; Müller, C.; Pace, G.; Friend, R. H.; Huck, W. T. S. *J. Am. Chem. Soc.* **2010**, *133*, 683.
(8) Hoven, C.; Yang, R.; Garcia, A.; Heeger, A. J.; Nguyen, T.-Q.; Bazan, G. C. *J. Am. Chem. Soc.* **2007**, *129*, 10976.
(9) He, Z.; Zhong, C.; Huang, X.; Wong, W.-Y.; Wu, H.; Chen, L.; Su, S.; Cao, Y. *Adv. Mater.* **2011**, *23*, 4636.
(10) Seo, J. H.; Gutacker, A.; Sun, Y.; Wu, H.; Huang, F.; Cao, Y.; Scherf, U.; Heeger, A. J.; Bazan, G. C. *J. Am. Chem. Soc.* **2011**, *133*, 8416.
(11) Seo, J. H.; Gutacker, A.; Walker, B.; Cho, S.; Garcia, A.; Yang, R.; Nguyen, T.-Q.; Heeger, A. J.; Bazan, G. C. *J. Am. Chem. Soc.* **2009**, *131*, 18220.
(12) Hoven, C. V.; Yang, R.; Garcia, A.; Crockett, V.; Heeger, A. J.; Bazan, G. C.; Nguyen, T.-Q. *Proc. Natl. Acad. Sci. U.S.A.* **2008**, *109*, 12730.
(13) Garcia, A.; Yang, R.; Jin, Y.; Walker, B.; Nguyen, T.-Q. *Appl. Phys. Lett.* **2007**, *91*, 153502.
(14) Garcia, A.; Bakus, R. C.; Zalar, P.; Hoven, C. V.; Brzezinski, J. Z.; Nguyen, T.-Q. *J. Am. Chem. Soc.* **2011**, *133*, 2492.
(15) Wu, A.; Yoo, D.; Lee, J. K.; Rubner, M. F. *J. Am. Chem. Soc.* **1999**, *121*, 4883.
(16) Rudmann, H.; Shimada, S.; Rubner, M. F. *J. Appl. Phys.* **2003**, *94*, 115.
(17) Lenes, M.; García-Belmonte, G.; Tordera, D.; Pertegás, A.; Bisquert, J.; Bolink, H. J. *Adv. Funct. Mater.* **2011**, *21*, 1581.
(18) Craciun, N. I.; Brondijk, J. J.; Blom, P. W. M. *Phys. Rev. B* **2008**, *77*, 035206.
(19) Nicolai, H. T.; Wetzelaer, G. A. H.; Kuik, M.; Kronemeijer, A. J.; de Boer, B.; Blom, P. W. M. *Appl. Phys. Lett.* **2010**, *96*, 172107.
(20) Seo, J. H.; Yang, R.; Brzezinski, J. Z.; Walker, B.; Bazan, G. C.; Nguyen, T.-Q. *Adv. Mater.* **2009**, *21*, 1006.
(21) Lampert, M. A.; Mark, P. *Current Injection in Solids*; Academic Press: New York, 1970.
(22) van Reenen, S.; Matyba, P.; Dzwilewski, A.; Janssen, R. A. J.; Edman, L.; Kemerink, M. *J. Am. Chem. Soc.* **2010**, *132*, 13776.
(23) Costa, R. D.; Ortí, E.; Bolink, H. J.; Monti, F.; Accorsi, G.; Armaroli, N. *Angew. Chem., Int. Ed.* **2012**, *51*, 8178.
(24) Pasveer, W. F.; Cottaar, J.; Tanase, C.; Coehoorn, R.; Bobbert, P. A.; Blom, P. W. M.; de Leeuw, D. M.; Michels, M. A. J. *Phys. Rev. Lett.* **2005**, *94*, 206601.
(25) Garcia, A.; Brzezinski, J. Z.; Nguyen, T.-Q. *J. Phys. Chem. C* **2009**, *113*, 2950.

dx.doi.org/10.1021/ja502055x | *J. Am. Chem. Soc.* XXXX, XXX, XXX−XXX